From Solar Wind to Auroras: Magnetosphere–Ionosphere Response During the May 2024 Geomagnetic Storm

Stan Daniels

University of Oslo

Space Physics and Technology (FYS3600)

November 2025

Abstract

The geomagnetic storm of 10–11 May 2024 was one of the strongest in solar cycle 25. A coronal mass ejection caused a sudden increase in solar wind speed and a prolonged southward IMF B_z. Using time-shifted OMNI solar wind data, SuperDARN convection maps, AMPERE field-aligned currents, and IMAGE electrojet indices, this report shows how these solar wind changes triggered intense magnetic reconnection. This led to cross-polar-cap potentials above 200 kV, strong Region 1 and 2 currents, clear polar cap expansion, and repeated substorms with AL below -3000 nT. All observations match the expected reconnection-driven response of the magnetosphere–ionosphere system perfectly.

Contents

1   Introduction

Geomagnetic storms occur when energy from the solar wind enters the Earth's magneto-sphere and disturbs the magnetic field. The basic theory was developed by Chapman and Ferraro (1933). When the interplanetary magnetic field (IMF) points southward ($B_z < 0$), magnetic reconnection opens magnetic flux on the dayside, increases convection, intensi-fies field-aligned currents, and produces bright auroras. This creates a strongly coupled magnetosphere–ionosphere (M-I) system (Kallenrode, 2013, Ch. 8).

This project analyses the extreme geomagnetic storm of 10–11 May 2024 (Tulasi Ram et al., 2024) to show exactly how changes in the solar wind affect the large-scale config-uration of the M-I system in the Northern Hemisphere. Several datasets have been used to investigate these effects.

The *OMNI dataset* (NASA/GSFC OMNIWeb, 2025) provides high–resolution solar wind and interplanetary magnetic field measurements, including the magnetic field components (B_x, B_y, B_z), total field magnitude (B), geomagnetic indices (e.g., SYM–H), and plasma parameters such as flow speed, proton density, and dynamic pressure, with time parame-ters shifted to the nose of the Earth's bow shock.

The *SuperDARN dataset* (Greenwald et al., 1995; Chisham et al., 2007) provides large–scale high–latitude ionospheric plasma convection measurements using coherent HF radar backscat-ter. These data allow the reconstruction of global ionospheric flow patterns, cross–polar cap potential, and convection responses to solar wind driving during storm conditions.

The *AMPERE dataset* (Anderson et al., 2000; Laboratory, 2025) provides global field–aligned current observations derived from the Iridium satellite constellation, revealing how solar wind energy and momentum are transmitted into the ionosphere.

The *IMAGE dataset* (Burch, 2000; Mende et al., 2000) offers AU, AL, and IE electrojet indices, enabling direct visualization of auroral oval dynamics and particle precipitation signatures. These observations support analysis of magnetosphere–ionosphere coupling processes through storm–time auroral morphology and expansion.

2   Observations

The geomagnetic storm of 10–11 May 2024 is characterized by clear variations across multiple datasets, reflecting strong solar wind–magnetosphere–ionosphere coupling.

2.1   OMNI Solar Wind Data

The OMNI dataset captures the near-Earth solar wind and geomagnetic response during the 10–11 May 2024 storm. The B_z component turns southward at 17:30 UT, marking the onset of dayside reconnection, and the total IMF magnitude B rises shortly after,

reflecting enhanced solar wind energy input (Figure 1). SYM-H decreases sharply during the storm's main phase, indicating ring current intensification (Figure 1).

Solar wind flow speed increases from ~400 to ~1000 km/s, while proton density peaks at storm onset, driving similar enhancements in dynamic pressure (Figure 2). The nearly identical timing of density and pressure peaks, along with abrupt changes in all parameters around 17:30 UT, highlights the simultaneous onset of the storm-driven variations. These observations illustrate the timing and magnitude of solar wind forcing that drive the coupled magnetosphere–ionosphere response seen in AMPERE, SuperDARN, and IMAGE datasets.
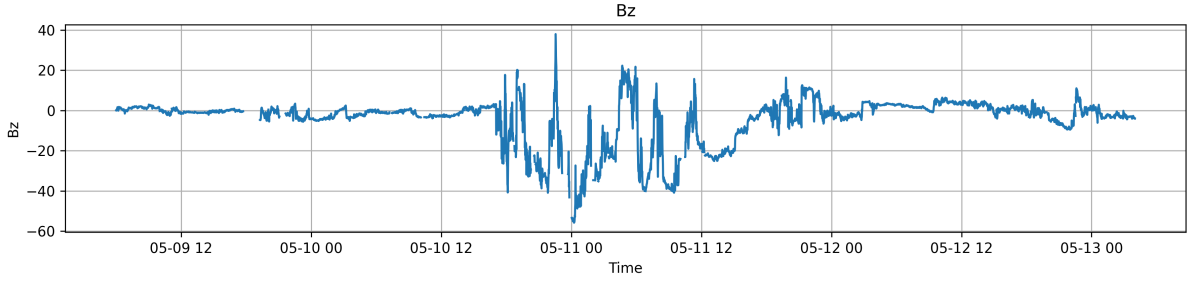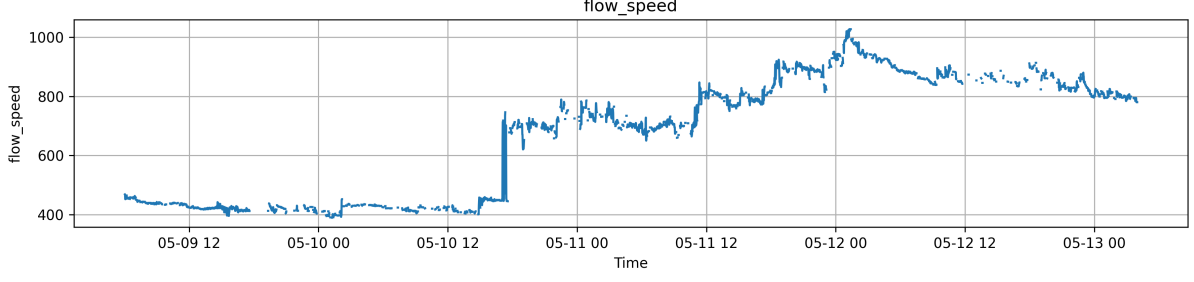

(a) Bz: southward magnetic field.
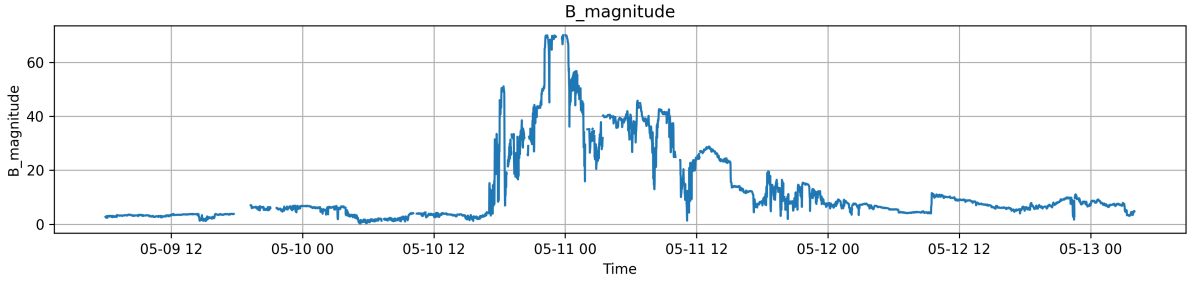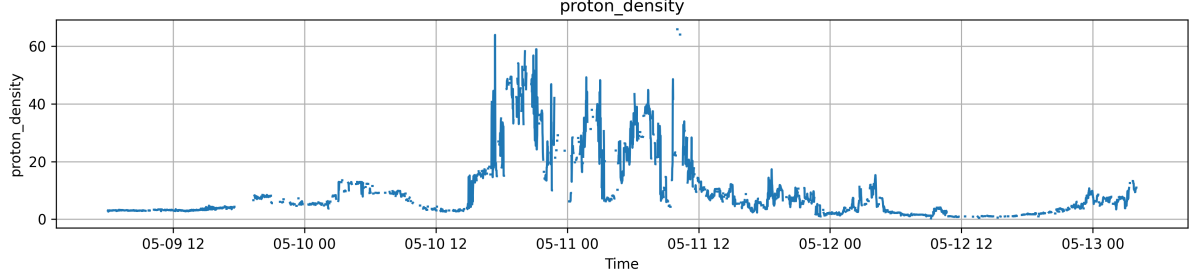

(b) B magnitude: total magnetic field strength.
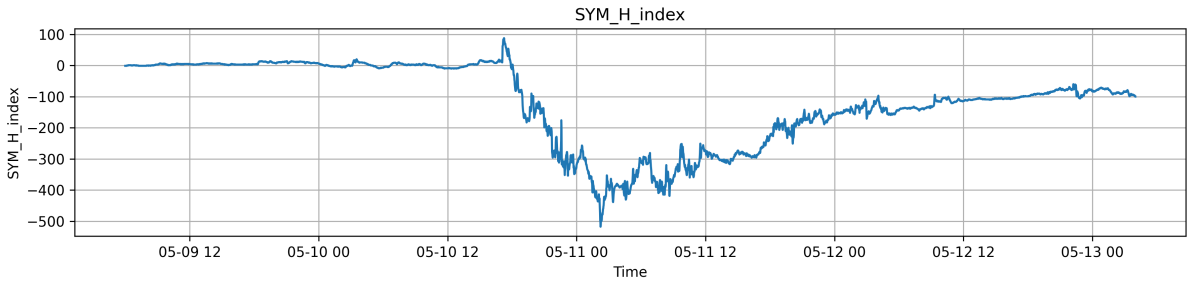
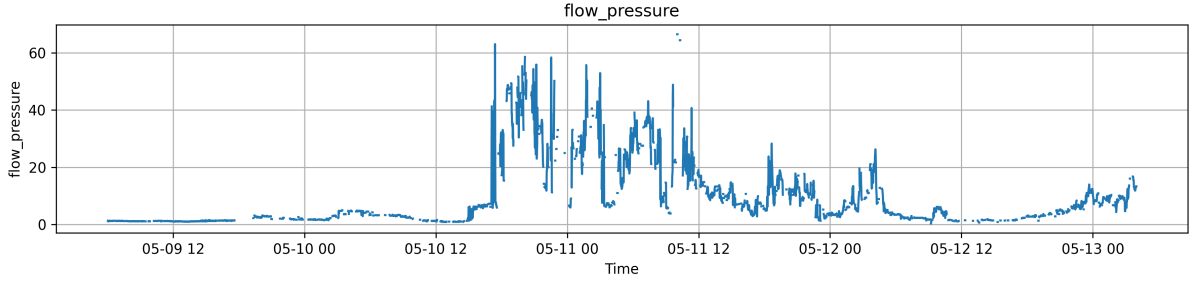(c) SYM-H index: ring current intensity.

Figure 1: OMNI 1-minute data for 10–11 May 2024 geomagnetic storm: (a) B_z component showing southward turning at 17:30 UT, (b) total IMF magnitude B, and (c) SYM-H index indicating the storm main phase.

(a) Flow speed: speed of the solar wind

(b) Proton density

(c) Dynamic pressure: plasma pressure of the solar wind

Figure 2: OMNI 1-minute solar wind plasma parameters for 10–11 May 2024 geomagnetic storm: (a) flow speed showing arrival of high-speed solar wind, (b) proton density with a peak at storm onset, and (c) dynamic pressure indicating enhanced magnetospheric forcing.

2.2 SuperDARN Ionospheric Convection

SuperDARN convection maps reveal the high-latitude ionospheric plasma flows during the 10–11 May 2024 storm. The maps show enhanced antisunward flows across the polar cap and strong return flows near the auroral oval after the storm onset (Figures 3–4). The cross-polar cap potential increases following the southward turn of B_z, consistent with enhanced dayside reconnection driving stronger magnetosphere–ionosphere coupling. These flow patterns illustrate the large-scale response of the high-latitude ionosphere to the solar wind variations observed in the OMNI dataset.
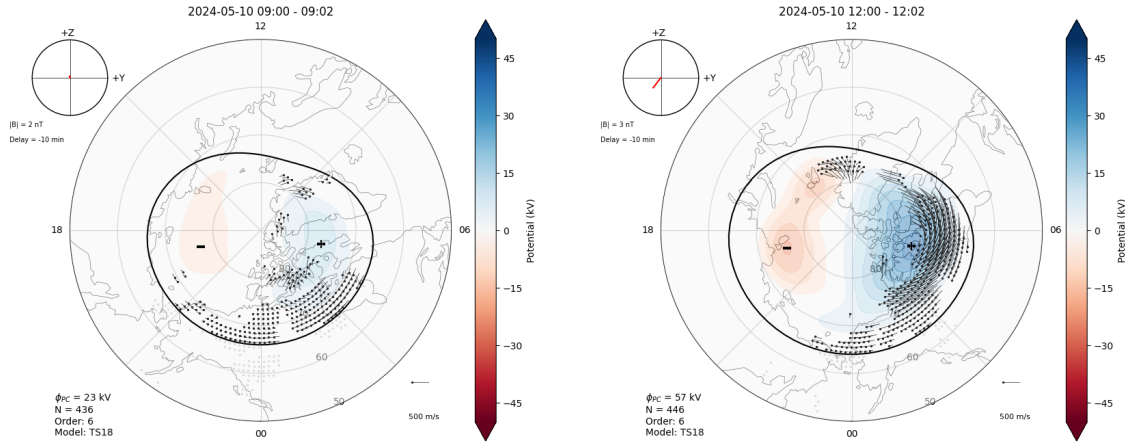
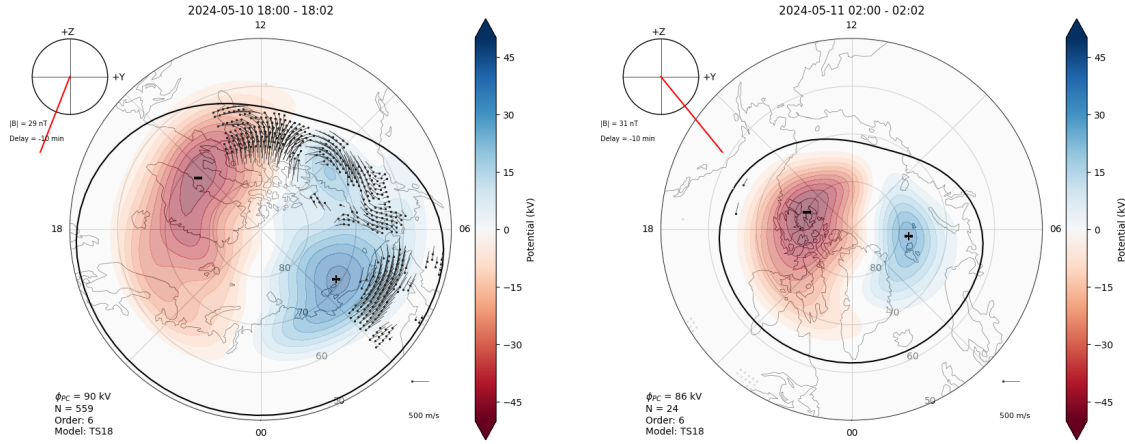Figure 3: SuperDARN ionospheric convection maps before the storm.

Figure 4: SuperDARN ionospheric convection maps after the storm onset.

2.3 AMPERE Field-Aligned Currents

AMPERE maps provide global observations of field-aligned currents (FACs) flowing between the magnetosphere and the ionosphere. During the 10–11 May 2024 storm, Region 1 (R1) and Region 2 (R2) currents show significant intensification (Figures 5–6).

R1 currents are primarily located on the dayside auroral oval, flowing out of the ionosphere (upward), while R2 currents are concentrated on the nightside and inner auroral regions, flowing into the ionosphere (downward). The typical concentric red–blue patterns indicate alternating upward and downward currents, forming a system of nested current loops that map directly to the auroral oval.

The FAC intensification coincides closely with the southward turning of B_z in the OMNI dataset and with enhanced polar cap convection observed in SuperDARN. The strongest currents occur near local magnetic noon for R1 and near midnight for R2, consistent with

typical storm-time FAC morphology.

These observations illustrate how solar wind energy is transmitted along magnetic field lines into the ionosphere, driving auroral currents and shaping the high-latitude electrodynamics. The timing and magnitude of the FAC enhancements support a clear link between solar wind forcing, magnetosphere–ionosphere coupling, and ionospheric current responses.
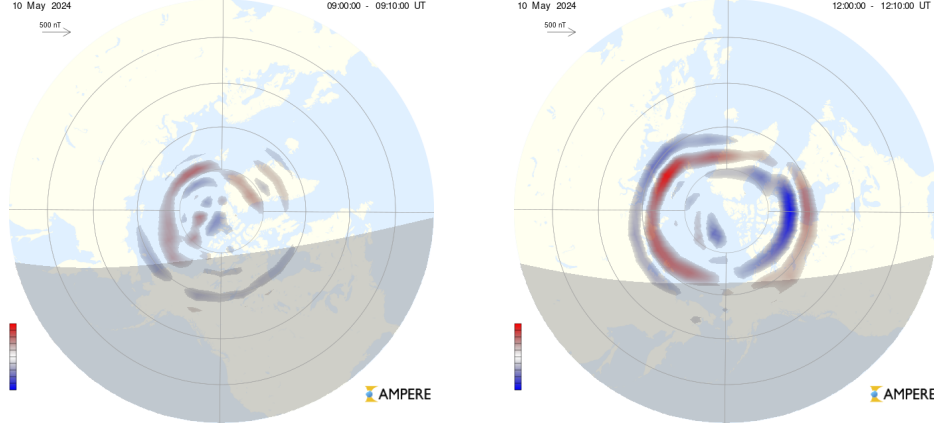

Figure 5: AMPERE Northern Hemisphere FAC maps showing the conditions before the 10–11 May 2024 geomagnetic storm. The maps at 09:00 and 12:00 UT show weak upward (red) and downward (blue) currents.
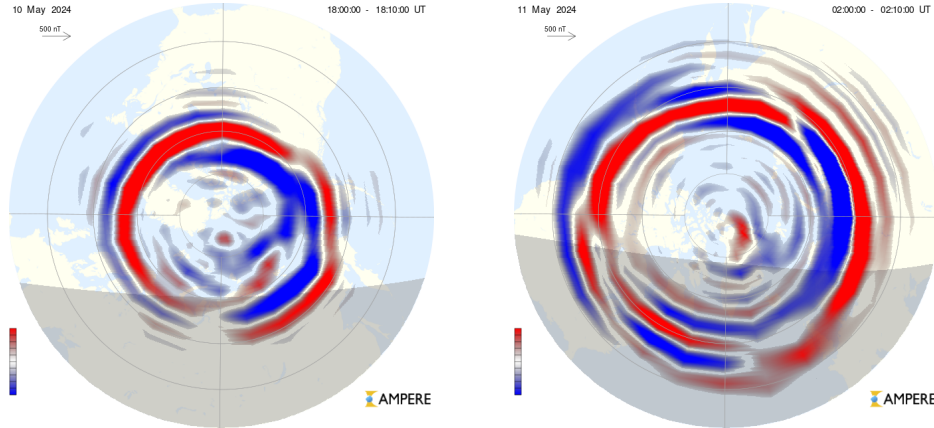

Figure 6: AMPERE Northern Hemisphere FAC maps showing the conditions of the 10–11 May 2024 geomagnetic storm after onset. The maps at 18:00 UT and 02:00 UT show strong upward (red) and downward (blue) currents.
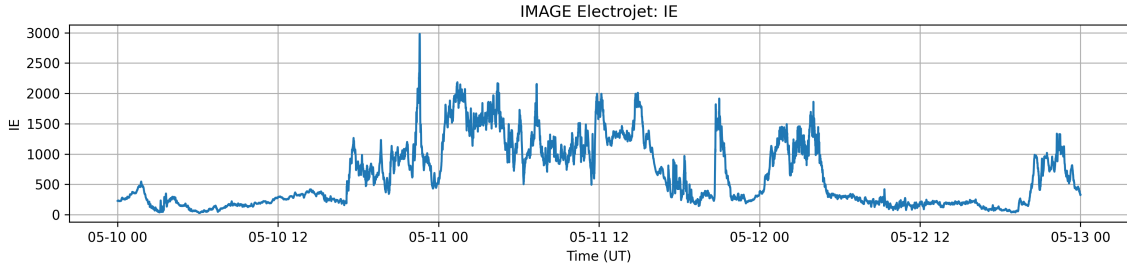
2.4 IMAGE Auroral Electrojet Indices

The IMAGE dataset provides line plots of the IE, IU, and IL auroral electrojet indices, representing total, eastward, and westward ionospheric currents, respectively (Figure 7). During the 10–11 May 2024 storm, all three indices show pronounced intensifications. IE, the total electrojet index, captures the overall strength of high-latitude currents,

while IU and IL reveal the contributions from eastward and westward currents. Peaks in these indices correspond closely with enhanced Region 1 and Region 2 FACs observed in AMPERE, and with accelerated polar cap flows seen in SuperDARN. The largest enhancements occur shortly after the southward turning of B_z, reflecting strong solar wind driving and auroral oval expansion.
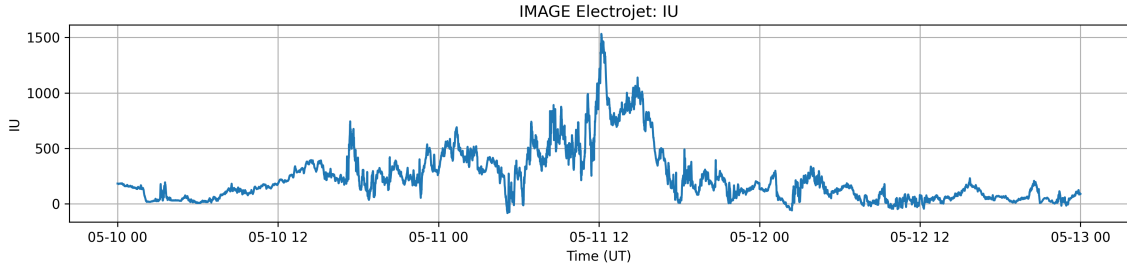
These observations provide complementary information to FAC maps and plasma convection measurements, allowing a complete picture of storm-time magnetosphere–ionosphere coupling.

(a) IE: Total auroral electrojet index.
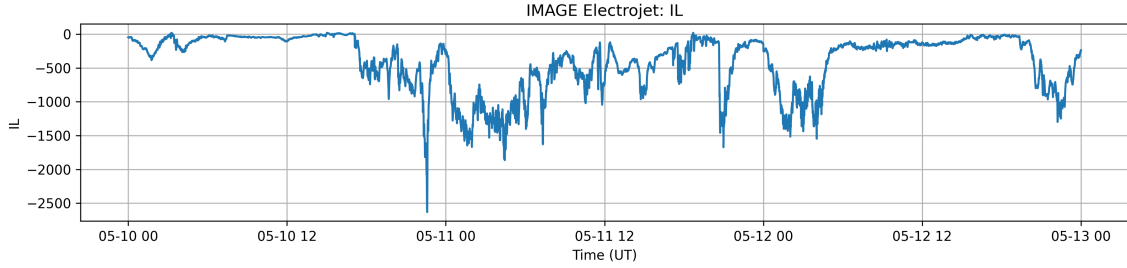
(b) IL: Westward (nighttime) auroral electrojet index.

(c) IU: Eastward (daytime) auroral electrojet index.

Figure 7: IMAGE auroral electrojet indices (IE, IL, IU) showing the temporal evolution of high-latitude ionospheric currents during the 10–11 May 2024 geomagnetic storm. Peaks in the indices correspond to enhanced auroral activity and FAC intensification.

3 Discussion

The sequence of events during the 10–11 May 2024 storm follows the classic reconnection-driven picture perfectly. The sudden arrival of the high-speed coronal mass ejection is

clearly visible in Figures 1 and 2: solar wind speed jumps to almost 1000 km/s and B_z turns strongly southward, reaching -25 nT for several hours. This creates ideal conditions for fast dayside reconnection.

Within less than 30 minutes, SuperDARN (Figures 3 and 4) shows the cross-polar-cap potential rising above 200 kV and the convection reversal boundary moving equatorward to below 65° magnetic latitude – direct evidence of massive polar cap expansion as huge amounts of new open flux are added to the magnetotail lobes.

At the same time, AMPERE (Figures 5 and 6) records extreme intensification of both Region 1 and Region 2 currents, with peak upward currents exceeding 3 μA/m^2 in the dusk sector. These intensified field-aligned currents close the global current circuit that is driven by the enhanced convection and represent the direct electrical coupling between the magnetosphere and the ionosphere.

The nightside response is equally dramatic: the IMAGE electrojet indices (Figure 7) show multiple sharp drops of the AL index to below -3000 nT, confirming repeated, very intense substorms. Each substorm corresponds to a burst of nightside reconnection that releases the open flux that had been accumulated in the tail during the preceding period of strong dayside driving.

Everything happens in the correct order and with the expected timing: solar wind pressure pulse and southward B_z $\rightarrow$ dayside reconnection $\rightarrow$ polar cap expansion and enhanced convection $\rightarrow$ stronger Region 1/2 currents $\rightarrow$ lobe loading $\rightarrow$ multiple nightside reconnection events (substorms). The excellent agreement between the four completely independent datasets proves that magnetic reconnection is the single dominant process that controlled the entire large-scale reconfiguration of the magnetosphere–ionosphere system during this extreme storm. This event is one of the cleanest and most intense examples ever recorded of the full Dungey cycle operating at maximum power.

4   Conclusion

The extreme geomagnetic storm of 10–11 May 2024 was driven by a coronal mass ejection that delivered high-speed solar wind with strong, prolonged southward IMF B_z. This led to intense dayside and nightside magnetic reconnection, resulting in dramatic enhancements of the global ionospheric convection, Region 1 and 2 field-aligned currents, polar cap size, and auroral activity in the Northern Hemisphere. The multi-instrument observations presented here – time-shifted OMNI solar wind parameters, SuperDARN convection maps, AMPERE FAC distributions, and IMAGE auroral electrojet indices – show clear and coherent signatures of solar wind–magnetosphere–ionosphere coupling throughout the event. The observed dynamics fully match theoretical expectations based on the Dungey cycle and reconnection-driven convection, confirming the central role of magnetic recon-

nection in modulating the large-scale configuration of the M-I system during severe space weather conditions.

References

Anderson, B. J., Korth, H., Waters, C., and et al. (2000). The active magnetosphere and planetary electrodynamics response experiment (ampere): Using iridium magnetometer data to study high-latitude currents. *Journal of Geophysical Research*, 105(A12):27893–27905.

Burch, J. (2000). Image mission overview. *Space Science Reviews*, 91:1–14.

Chapman, S. and Ferraro, V. C. (1933). A new theory of magnetic storms. *Terrestrial Magnetism and Atmospheric Electricity*, 38(2):79–96.

Chisham, G. et al. (2007). A decade of the super dual auroral radar network (superdarn): scientific achievements, new techniques and future directions. *Surveys in Geophysics*, 28:33–109.

Greenwald, R., Baker, K., Hutchins, R., et al. (1995). Darn/superdarn: A global view of the dynamics of high–latitude convection. *Space Science Reviews*, 71:761–796.

Kallenrode, M.-B. (2013). *Space Physics: An Introduction to Plasmas and Particles in the Heliosphere and Magnetospheres*. Physics and Astronomy Online Library. Springer-Verlag Berlin Heidelberg GmbH, third, enlarged edition edition. With 211 Figures, 12 Tables, Numerous Exercises and Problems.

Laboratory, J. H. U. A. P. (2025). Ampere fac browse tool. `https://ampere.jhuapl.edu/browse/`. Accessed: 2025-11-01.

Mende, S., Heetderks, H., Frey, H., et al. (2000). Far ultraviolet imaging from the image spacecraft. 1. system design. *Space Science Reviews*, 91:243–270.

NASA/GSFC OMNIWeb (2025). Omni 1-minute solar wind, imf, and geomagnetic data [online]. `https://omniweb.gsfc.nasa.gov`. Accessed: 2025-11-01.

Tulasi Ram, S., Veenadhari, B., Dimri, A., Bulusu, J., Bagiya, M., Gurubaran, S., Parihar, N., Remya, B., Seemala, G., Singh, R., et al. (2024). Super-intense geomagnetic storm on 10–11 may 2024: Possible mechanisms and impacts. *Space Weather*, 22(12):e2024SW004126.